

Generalized Coprime Array Configurations for Direction-of-Arrival Estimation

Si Qin, Yimin D. Zhang, *Senior Member, IEEE*, and Moeness G. Amin, *Fellow, IEEE*

Abstract—A coprime array uses two uniform linear subarrays to construct an effective difference coarray with certain desirable characteristics, such as a high number of degrees-of-freedom for direction-of-arrival (DOA) estimation. In this paper, we generalize the coprime array concept with two operations. The first operation is through the compression of the inter-element spacing of one subarray and the resulting structure treats the existing variations of coprime array configurations as well as the nested array structure as its special cases. The second operation exploits two displaced subarrays, and the resulting coprime array structure allows the minimum inter-element spacing to be much larger than the typical half-wavelength requirement, making them useful in applications where a small interelement spacing is infeasible. The performance of the generalized coarray structures is evaluated using their difference coarray equivalence. In particular, we derive the analytical expressions for the coarray aperture, the achievable number of unique lags, and the maximum number of consecutive lags for quantitative evaluation, comparison, and design of coprime arrays. The usefulness of these results is demonstrated using examples applied for DOA estimations utilizing both subspace-based and sparse signal reconstruction techniques.

Index Terms—Compressive sensing, coprime array, difference coarray, direction-of-arrival estimation, nested array.

I. INTRODUCTION

DIRECTION-OF-ARRIVAL (DOA) estimation, which determines the spatial spectra of the impinging electromagnetic waves, is an important application area of antenna arrays. It is well known that conventional subspace-based DOA estimation methods, such as MUSIC and ESPRIT [3], [4], resolve up to $N - 1$ sources with an N -element array. However, the problem of detecting more sources than the number of sensors is of tremendous interest in various applications [5], [6]. Toward this purpose, a higher number of degrees-of-freedom

(DOFs) is usually achieved by exploiting a sparse array under the coarray equivalence. For example, the minimum redundancy array (MRA) [7] is a linear array structure that, for a given number of physical sensors, maximizes the number of consecutive virtual sensors in the resulting difference coarray. The minimum hole array (also known as the Golomb array) minimizes the number of holes in the difference coarray [8]. However, there are no general expressions for the MRA and Golomb array configurations as well as the achievable DOFs for an arbitrary number of sensors. Therefore, the optimum design and performance analysis of such arrays are not easy in general. In addition, finding the suitable covariance matrix corresponding to a large array requires a rather complicated time-consuming iterative process.

Recently, several array configurations have been proposed as attractive alternatives for sparse array construction. The nested array [9], which is obtained by combining two uniform linear subarrays, in which one subarray has a unit inter-element spacing, can resolve $O(N^2)$ sources with N sensors. Unlike the MRA, the nested array configuration is easy to construct and it is possible to obtain the exact expressions of the sensor locations and the available DOFs for a given number of the sensors. The total aperture and the number of unique and consecutive coarray sensors can be subsequently obtained [9]. Note that, as some of the sensors in a nested array are closely located, the mutual coupling effects between antennas may become significant and thus compromise the coarray reconstruction capability and the DOA estimation performance [10], [11]. The recently developed coprime array [12], which is referred to as the prototype coprime array in this paper, utilizes a coprime pair of uniform linear subarrays, where one is of M sensors with an inter-element spacing of N units, whereas the other is of N elements with an inter-element spacing of M units. By choosing the integer numbers M and N to be coprime, a coprime array can resolve $O(MN)$ sources with $M + N - 1$ sensors. This is attractive when it is necessary to reduce mutual coupling between elements. A different coprime array structure was proposed in [13] by extending the number of elements in one subarray. The result is a larger number of consecutive virtual sensors under the coarray equivalence. By considering the difference coarray of $N + 2M - 1$ sensors, they demonstrated that continuous correlation lags can be created from $-MN$ to MN .

A close examination of the extended coprime configuration reveals that there is at least one pair of adjacent sensors that is separated only by the unit spacing, which is typically half wavelength to avoid the grating lobe problem. In addition to the mutual coupling effect as described above, there are situations that such half-wavelength minimum spacing is infeasible or impractical. One of the examples is when the physical size of the

Manuscript received July 03, 2014; revised November 06, 2014; accepted January 03, 2015. Date of publication January 16, 2015; date of current version February 11, 2015. The associate editor coordinating the review of this manuscript and approving it for publication was Dr. Pengfei Xia. The work was supported in part by the Office of Naval Research under Grant No. N00014-13-1-0061. Part of the results was presented at the IEEE International Conference on Acoustics, Speech, and Signal Processing (ICASSP), Florence, Italy, May 2014 [1], and the IEEE Sensor Array and Multichannel Signal Processing Workshop, A Coruña, Spain, June 2014 [2].

The authors are with Wireless Communications and Positioning Laboratory, Center for Advanced Communications, Villanova University, PA 19085 USA (e-mail: yimin.zhang@villanova.edu).

Color versions of one or more of the figures in this paper are available online at <http://ieeexplore.ieee.org>.

Digital Object Identifier 10.1109/TSP.2015.2393838

antenna sensors is larger than half-wavelength (e.g., [14]). Indeed, many parabola antennas are designed to have a large size for enhanced directivity [15]. This problem is alleviated through an effective array configuration design in which the minimum inter-element spacing is much larger than the typical half-wavelength requirement [1].

In this paper, we propose the generalization of the coprime array concept, which comprises two operations. The first operation is the compression of the inter-element spacing of one constituting subarray in the coprime array by a positive integer. The resulting coarray structure is referred to as *coprime array with compressed inter-element spacing (CACIS)*. As such, the coprime array structure developed in [13], which doubles the number of sensors in a constituting subarray, becomes a special case of the proposed CACIS structure. The second operation introduces a displacement between the two subarrays, yielding a *coprime array with displaced subarrays (CADiS)*. The resulting CADiS structure allows the minimum inter-element spacing to be much larger than the typical half-wavelength requirement. These two operations can be performed separately or jointly. We evaluate the performance of each individual generalized coarray structure corresponding to these operations using their respective difference coarray equivalence. In particular, we derive the analytical expressions of the coarray aperture, the achievable number of unique lags, and the maximum number of consecutive lags for quantitative evaluation, comparison, and optimal design.

It is noted that the focus of this paper is the examination of the generalized coprime array structures in the context of narrowband DOA estimation. Wideband or multi-frequency signals may further permit the utilization of frequency-domain DOFs for enhanced DOA estimation capability. For example, it is shown in [16] that coprime arrays that handle wideband signals can benefit from frequency diversity to achieve improved DOA estimation performance. On the other hand, the exploitation of two coprime frequencies in a uniform linear array can generate an equivalent coprime array with an increased number of DOFs [17], [18].

The rest of the paper is organized as follows. In Section II, we first review the coprime array concept based on the difference coarray concept. Then two different DOA estimation approaches, which are respectively based on the MUSIC algorithm and compressive sensing (CS) techniques, exploiting coprime arrays are summarized in Section III. The two generalized coprime array structures, i.e., CACIS and CADiS, are respectively described in Sections IV and V with the analytical expressions of array aperture, unique coarray lags, and consecutive coarray lags. Different nested array structures are clarified and compared in Section VI. Simulation results are provided in Section VII to numerically compare the performance of the different generalized coprime array configurations with the two DOA estimation techniques. Such results reaffirm and demonstrate the usefulness of the results presented in Sections IV and V. Section VIII concludes this paper.

Notations: We use lower-case (upper-case) bold characters to denote vectors (matrices). In particular, \mathbf{I}_N denotes the $N \times N$ identity matrix. $(\cdot)^*$ implies complex conjugation, whereas $(\cdot)^T$ and $(\cdot)^H$ respectively denote the transpose and conjugate transpose of a matrix or vector. $\text{vec}(\cdot)$ denotes the vectorization operator that turns a matrix into a vector by stacking all columns on

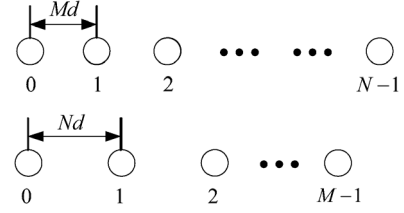


Fig. 1. The prototype coprime array configuration.

top of the another, and $\text{diag}(\mathbf{x})$ denotes a diagonal matrix that uses the elements of \mathbf{x} as its diagonal elements. $\|\cdot\|_2$ and $\|\cdot\|_1$ respectively denote the Euclidean (l_2) and l_1 norms, and $\mathbb{E}(\cdot)$ is the statistical expectation operator. \otimes denotes the Kronecker product, and $\text{real}(\cdot)$ and $\text{imag}(\cdot)$ represent the real and imaginary part operations. $\mathcal{CN}(\mathbf{a}, \mathbf{B})$ denotes joint complex Gaussian distribution with mean vector \mathbf{a} and covariance matrix \mathbf{B} .

II. COPRIME ARRAY CONCEPT

A. Prototype Coprime Array Structure

A prototype coprime array [12], as described in the previous section, is illustrated in Fig. 1, where M and N are coprime integers. Without loss of generality, we assume $M < N$. The unit inter-element spacing d is set to $\lambda/2$, where λ denotes the wavelength. The array sensors are positioned at

$$\mathbb{P} = \{Mnd | 0 \leq n \leq N-1\} \cup \{Nmd | 0 \leq m \leq M-1\}. \quad (1)$$

Because the two subarrays share the first sensor at the zeroth position, the total number of the sensors used in the coprime array is $M + N - 1$. Note that the minimum inter-element spacing in this coprime array is $\lambda/2$.

Denote $\mathbf{p} = [p_1, \dots, p_{M+N-1}]^T$ as the positions of the array sensors where $p_i \in \mathbb{P}$, $i = 1, \dots, M + N - 1$, and the first sensor is assumed as the reference, i.e., $p_1 = 0$. Assume that Q uncorrelated signals impinging on the array from angles $\Theta = [\theta_1, \dots, \theta_Q]^T$, and their discretized baseband waveforms are expressed as $s_q(t)$, $t = 1, \dots, T$, for $q = 1, \dots, Q$. Then, the data vector received at the coprime array is expressed as,

$$\mathbf{x}(t) = \sum_{q=1}^Q \mathbf{a}(\theta_q) s_q(t) + \mathbf{n}(t) = \mathbf{A} \mathbf{s}(t) + \mathbf{n}(t), \quad (2)$$

where

$$\mathbf{a}(\theta_q) = \left[1, e^{j \frac{2\pi p_2}{\lambda} \sin(\theta_q)}, \dots, e^{j \frac{2\pi p_{M+N-1}}{\lambda} \sin(\theta_q)} \right]^T \quad (3)$$

is the steering vector of the array corresponding to θ_q , $\mathbf{A} = [\mathbf{a}(\theta_1), \dots, \mathbf{a}(\theta_Q)]$, and $\mathbf{s}(t) = [s_1(t), \dots, s_Q(t)]^T$. The elements of the noise vector $\mathbf{n}(t)$ are assumed to be independent and identically distributed (i.i.d.) random variables following the complex Gaussian distribution $\mathcal{CN}(0, \sigma_n^2 \mathbf{I}_{M+N-1})$.

The covariance matrix of data vector $\mathbf{x}(t)$ is obtained as

$$\begin{aligned} \mathbf{R}_{\mathbf{x}\mathbf{x}} &= \mathbb{E}[\mathbf{x}(t)\mathbf{x}^H(t)] = \mathbf{A} \mathbf{R}_{\mathbf{s}\mathbf{s}} \mathbf{A}^H + \sigma_n^2 \mathbf{I}_{M+N-1} \\ &= \sum_{q=1}^Q \sigma_q^2 \mathbf{a}(\theta_q) \mathbf{a}^H(\theta_q) + \sigma_n^2 \mathbf{I}_{M+N-1}, \end{aligned} \quad (4)$$

where $\mathbf{R}_{\mathbf{s}\mathbf{s}} = \mathbb{E}[\mathbf{s}(t)\mathbf{s}^H(t)] = \text{diag}([\sigma_1^2, \dots, \sigma_Q^2])$ is the source covariance matrix, with σ_q^2 denoting the input signal power of

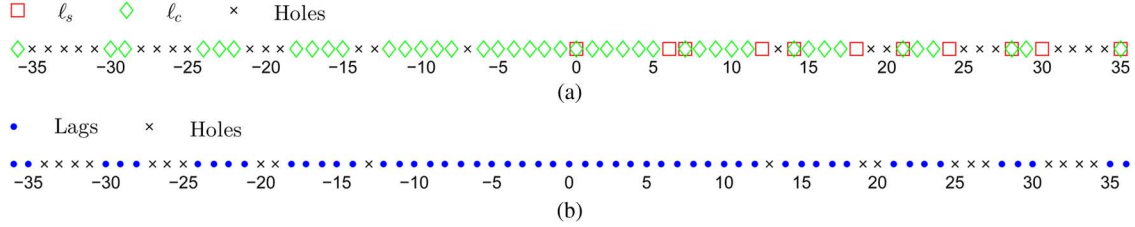


Fig. 2. An example of prototypal coprime configuration coarrays, where $M = 6$ and $N = 7$. (a) The set L_s and L_c . (b) The lag positions in full set L_P .

the q th source, $q = 1, \dots, Q$. In practice, the covariance matrix is estimated using the T available samples, i.e.,

$$\hat{\mathbf{R}}_{\mathbf{x}\mathbf{x}} = \frac{1}{T} \sum_{t=1}^T \mathbf{x}(t)\mathbf{x}^H(t). \quad (5)$$

From a pair of antennas located at the i th and k th positions in \mathbf{p} , the correlation $E[x_i(t)x_k^*(t)]$ yields the (i, k) th entry in $\mathbf{R}_{\mathbf{x}\mathbf{x}}$ with lag $p_i - p_k$. As such, all the available values of i and k , where $0 \leq i \leq M + N - 1$ and $0 \leq k \leq M + N - 1$, yield virtual sensors of the following difference coarray:

$$\mathbb{C}_P = \{\mathbf{z} \mid \mathbf{z} = \mathbf{u} - \mathbf{v}, \mathbf{u} \in \mathbb{P}, \mathbf{v} \in \mathbb{P}\}. \quad (6)$$

The significance of the difference coarray is that the correlation of the received signal can be calculated at all differences in set \mathbb{C}_P . Any application which depends only on such correlation (e.g., DOA estimation) can exploit all the DOFs offered by the resulting coarray structure. Using a part or the entire set of the distinct auto-correlation terms in set \mathbb{C}_P , instead of the original array, to perform DOA estimation, we can increase the number of detectable sources by the array. The maximum number of the DOFs is determined by the number of unique elements in the following set

$$L_P = \{l_P \mid l_P d \in \mathbb{C}_P\}. \quad (7)$$

To gain more insights about the difference coarrays, we separately consider the self-differences of the two subarrays and their cross-differences. Since the coarray is obtained from the Hermitian matrix $\mathbf{R}_{\mathbf{x}\mathbf{x}}$, the self-difference in the coarray has positions

$$L_s = \{l_s \mid l_s = Mn\} \cup \{l_s \mid l_s = Nm\}, \quad (8)$$

and the corresponding mirrored positions $L_s^- = \{-l_s \mid l_s \in L_s\}$, whereas the cross-difference has positions

$$L_c = \{l_c \mid l_c = Nm - Mn\}, \quad (9)$$

and the corresponding mirrored positions $L_c^- = \{-l_c \mid l_c \in L_c\}$, for $0 \leq n \leq N - 1$ and $0 \leq m \leq M - 1$. Consequently, the full set of lags in the virtual array is given by,

$$L_P = L_s \cup L_s^- \cup L_c \cup L_c^-. \quad (10)$$

An example is illustrated in Fig. 2, where $M = 6$ and $N = 7$. Fig. 2(a) show the self- and cross-lags described in (8) and (9). If we include the negative mirror of the above set, then the full set of lags becomes symmetric, as shown in Fig. 2(b). Notice that

some ‘‘holes’’, e.g., $\pm 13, \pm 19, \pm 20$, still exist in the difference coarray and are indicated by \times in this figure. The total number of lags in the symmetric set gives a global upper bound of the achievable DOFs.

III. DOA ESTIMATION TECHNIQUES

To better understand the significance of the performance metrics to be examined, i.e., the coarray aperture, the number of consecutive coarray lags, and the number of unique lags of coarray lags, we briefly review the two representative DOA estimation techniques that are recently developed for coprime array configurations. The first one is based on the well-known MUSIC algorithm, and the spatial smoothing technique [19]–[21] is applied to construct a suitable covariance matrix from the virtual sensor output prior to performing MUSIC spectrum estimation [12], [13]. Notice that, while the use of virtual sensors substantially increases the available number of DOFs, the application of spatial smoothing essentially halves the number of available virtual sensors. A different approach to perform DOA estimation exploiting coprime arrays is through sparse signal reconstruction by taking advantages of the fact that the spatial signal spectra are sparse. Such sparse signal reconstruction is achieved using the recently developed compressive sensing techniques [22], [23]. These two DOA estimation techniques are summarized below.

A. MUSIC Algorithm

Vectorizing $\mathbf{R}_{\mathbf{x}\mathbf{x}}$ in (4) yields

$$\mathbf{z} = \text{vec}(\mathbf{R}_{\mathbf{x}\mathbf{x}}) = \tilde{\mathbf{A}}\mathbf{b} + \sigma_n^2 \tilde{\mathbf{I}} = \mathbf{B}\mathbf{r}, \quad (11)$$

where $\tilde{\mathbf{A}} = [\tilde{\mathbf{a}}(\theta_1), \dots, \tilde{\mathbf{a}}(\theta_Q)]$, $\tilde{\mathbf{a}}(\theta_q) = \mathbf{a}^*(\theta_q) \otimes \mathbf{a}(\theta_q)$, $\mathbf{b} = [\sigma_1^2, \dots, \sigma_Q^2]^T$, $\tilde{\mathbf{I}} = \text{vec}(\mathbf{I}_{M+N-1})$. In addition, $\mathbf{B} = [\tilde{\mathbf{A}}, \tilde{\mathbf{I}}]$ and $\mathbf{r} = [\mathbf{b}^T, \sigma_n^2]^T = [\sigma_1^2, \dots, \sigma_Q^2, \sigma_n^2]$ are used for notational simplicity. The vector \mathbf{z} amounts to the received data from a virtual array with an extended coarray aperture whose corresponding steering matrix is defined by $\tilde{\mathbf{A}}$. However, the virtual source signal becomes a single snapshot of \mathbf{b} . In addition, the rank of the noise-free covariance matrix of \mathbf{z} , $\mathbf{R}_{\mathbf{z}\mathbf{z}} = \mathbf{z}\mathbf{z}^H$, is one. As such, the problem is similar to handling fully coherent sources, and subspace-based DOA estimation techniques, such as MUSIC, fail to yield reliable DOA estimates when multiple signals impinge to the array.

To overcome this problem, it is proposed in [13] to apply spatial smoothing technique to the covariance matrix so that its rank can be restored. Since spatial smoothing requires a consecutive difference lag set so that every subarray has similar manifold, we extract all the consecutive lag samples of \mathbf{z} and form a new

vector \mathbf{z}_1 . Denote $[-l_\xi, l_\xi]$ as the consecutive lag range in \mathbb{L}_P . Then, \mathbf{z}_1 can be expressed as

$$\mathbf{z}_1 = \tilde{\mathbf{A}}_1 \mathbf{b} + \sigma_n^2 \tilde{\mathbf{I}}_1, \quad (12)$$

where $\tilde{\mathbf{A}}_1$ is identical to the manifold of a uniform linear array (ULA) with $2l_\xi + 1$ sensors located from $-l_\xi d$ to $l_\xi d$ and $\tilde{\mathbf{I}}_1$ is a $(2l_\xi + 1) \times 1$ vector of all zeros except a 1 at the $(l_\xi + 1)$ th position. We divide this virtual array into $l_\xi + 1$ overlapping subarrays, \mathbf{z}_{1i} , $i = 1, \dots, l_\xi + 1$, each with $l_\xi + 1$ elements, where the i th subarray has sensors located at $(-i + 1 + k)d$, with $k = 0, 1, \dots, l_\xi$ denoting the index of the overlap subarray used in the spatial smoothing.

Define

$$\mathbf{R}_i = \mathbf{z}_{1i} \mathbf{z}_{1i}^H. \quad (13)$$

Taking the average of \mathbf{R}_i over all i , we obtain

$$\mathbf{R}'_{zz} = \frac{1}{l_\xi + 1} \sum_{i=1}^{l_\xi + 1} \mathbf{R}_i, \quad (14)$$

which yields a full-rank covariance matrix so that the MUSIC algorithm can be performed for DOA estimation directly. As a result, l_ξ DOFs are achieved, which are roughly equal to half of the available consecutive lags of the resulting coarray.

B. Compressive Sensing Approach

Alternatively, (11) can be solved using the CS approach [23]. The desired result of \mathbf{b} , whose elements are the first Q entries of vector \mathbf{r} , can be obtained from the solution to the following constrained l_0 -norm minimization problem

$$\hat{\mathbf{r}}^\circ = \arg \min_{\mathbf{r}^\circ} \|\mathbf{r}^\circ\|_0 \quad \text{s.t.} \quad \|\mathbf{z} - \mathbf{B}^\circ \mathbf{r}^\circ\|_2 < \epsilon, \quad (15)$$

where ϵ is a user-specific bound, \mathbf{B}° is a sensing matrix consisting of the searching steering vectors and $\hat{\mathbf{i}}$, whereas \mathbf{r}° is the sparse entries in these search grids to be determined. The sensing matrix \mathbf{B}° and the entry vector \mathbf{r}° are defined over a finite grid $\theta_1^g, \dots, \theta_G^g$, where $G \gg Q$. The last entry of \mathbf{r}° denotes the estimate of σ_n^2 , whereas the positions and values of the non-zero entries in the other elements of \mathbf{r}° represent the estimated DOAs and the corresponding signal power.

This type of problems has been the objective of intensive studies in the area of CS, and a number of effective numerical computation methods have been developed [24]–[28]. In [23], the batch Lasso method was used, but other methods may also be used. The objective function of the Lasso algorithm is defined as

$$\hat{\mathbf{r}}^\circ = \arg \min_{\mathbf{r}^\circ} \left[\frac{1}{2} \|\mathbf{z} - \mathbf{B}^\circ \mathbf{r}^\circ\|_2 + \lambda_t \|\mathbf{r}^\circ\|_1 \right], \quad (16)$$

where the l_2 norm in the objective function denotes the ordinary least-squares (OLS) cost function, and the l_1 norm involves the sparsity constraint. In addition, λ_t is a penalty parameter which can be tuned to trade off the OLS error for the number of nonzero entries (degree of sparsity) in the estimates [24]. The above Lasso objective is convex in \mathbf{r}° , and can be optimized using linear programming techniques [29].

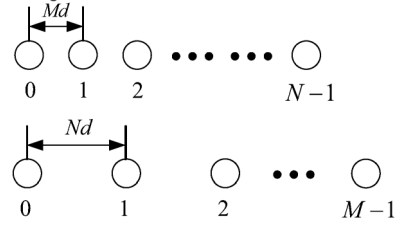


Fig. 3. The CACIS configuration.

IV. COPRIME ARRAY WITH COMPRESSED INTER-ELEMENT SPACING

Now we present our main results that generalize coarray structures in two operations, i.e., CACIS and CADiS. The CACIS is presented in this section, whereas the CADiS is examined in the following section.

We consider two subarrays with M and N sensors, where M and N are coprime. Note that, in the sequel, the condition that $M < N$ is no longer assumed. Unlike the prototype coprime array, an integer compression factor p is introduced for changing the inter-element spacing of one subarray. Assume that M can be expressed as a product of two positive integers p and \check{M} , i.e.,

$$M = p\check{M}, \quad (17)$$

for some p that takes a value between 2 and M . It is easy to confirm that \check{M} and N are also coprime since M and N do not have common factors other than unity. As shown in Fig. 3, in the generalized coprime array, the M -element subarray has an inter-element spacing of Nd , whereas the N -element subarray has an inter-element space of $\check{M}d = Md/p$. As such, the generalized coprime array can be considered that the inter-element spacing of one constituting subarray is compressed by an integer factor of p , thus comes the term of coprime array with compressed inter-element spacing (CACIS). Note that all arrays consist of the same $M + N - 1$ physical antenna sensors and their aperture is $(M - 1)N$, regardless the value of p . It is shown that the variation of the coprime array configuration used in [13] is a special case of the CACIS configuration by choosing $p = 2$.

In this array configuration, the self-lags of the two subarrays are given by the following set¹,

$$\tilde{\mathbb{L}}_s = \{\tilde{l}_s | \tilde{l}_s = \check{M}n\} \cup \{\tilde{l}_s | \tilde{l}_s = Nm\}, \quad (18)$$

and the corresponding mirrored positions $\tilde{\mathbb{L}}_s^-$, whereas the cross-lags between the two subarrays are given by

$$\tilde{\mathbb{L}}_c = \{\tilde{l}_c | \tilde{l}_c = Nm - \check{M}n\}, \quad (19)$$

and the corresponding $\tilde{\mathbb{L}}_c^-$, where $0 \leq m \leq M - 1$ and $0 \leq n \leq N - 1$.

To completely exploit the DOFs of the CACIS configuration, we summarize the properties of $\tilde{\mathbb{L}}_s$ and $\tilde{\mathbb{L}}_c$ in the following proposition.

Proposition 1: The following facts hold for the CACIS:

- There are MN distinct integers in set $\tilde{\mathbb{L}}_c$.
- $\tilde{\mathbb{L}}_c$ contains all the contiguous integers in the range $-(N - 1) \leq \tilde{l}_c \leq MN - \check{M}(N - 1) - 1$.

¹($\tilde{\cdot}$) is used to emphasize variables corresponding to the CACIS structure.

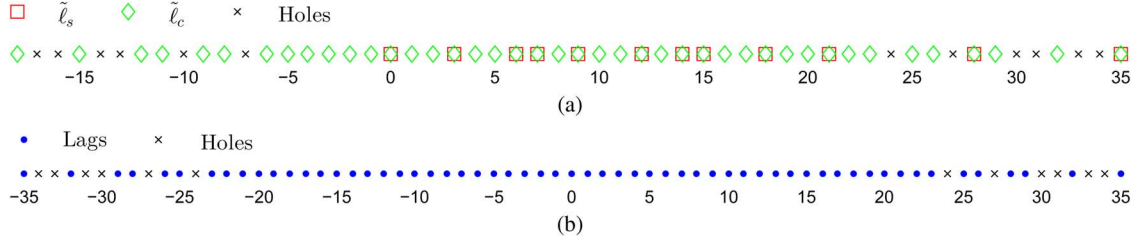


Fig. 4. An example of CACIS configuration coarrays, where $\check{M} = 3$, $p = 2$ and $N = 7$. (a) The set $\check{\mathbb{L}}_s$ and $\check{\mathbb{L}}_c$. (b) The full set $\check{\mathbb{L}}_P$.

- (c) The negative values form a subset of the flipped positive values in set $\check{\mathbb{L}}_c$, i.e., $\{\check{l}_c | \check{l}_c < 0, \check{l}_c \in \check{\mathbb{L}}_c\} \subseteq \{-\check{l}_c | \check{l}_c > 0, \check{l}_c \in \check{\mathbb{L}}_c\}$.
- (d) The self-lags form a subset of the cross-lags, i.e., $(\check{\mathbb{L}}_s^- \cup \check{\mathbb{L}}_s^+) \subseteq (\check{\mathbb{L}}_c^- \cup \check{\mathbb{L}}_c^+)$.
- (e) There are ‘‘holes’’ located at both positive range and negative ranges of $\check{\mathbb{L}}_c$. The holes falling in the negative range are located at $-(a\check{M} + bN)$, where $a \geq 0$, $b > 0$ are integers.

The proof is provided in Appendix I.

Based on the properties (c) and (d) of Proposition 1, the entire lag set in the virtual array defined in (10) consists of $\{\check{l}_c | \check{l}_c \geq 0, \check{l}_c \in \check{\mathbb{L}}_c\} \cup \{-\check{l}_c | \check{l}_c \geq 0, \check{l}_c \in \check{\mathbb{L}}_c\}$, thus resulting in Proposition 2.

Proposition 2: The CACIS configuration defined in equation (17) yields a virtual array such that:

- (a) It contains $2MN - (\check{M} + 1)(N - 1) - 1$ unique lags of virtual sensors.
- (b) Among the unique lags, there are $2MN - 2\check{M}(N - 1) - 1$ consecutive integers within the range $[-MN + \check{M}(N - 1) + 1, MN - \check{M}(N - 1) - 1]$.

The proof is provided in Appendix II. In Fig. 4, $M = 2\check{M}$ is considered as an illustrative example of above properties. It is equivalent to the configuration proposed in [13]. In this case, the virtual array consists of $3\check{M}N + \check{M} - N$ unique lags, among which $[-MN - \check{M} + 1, MN + \check{M} - 1]$ are consecutive. Note that our result contains more consecutive lags and is more precise than the result provided in [13], which is $[-\check{M}N + 1, \check{M}N - 1]$. The difference, which is based on property (b) of Proposition 1, is clarified in Appendix I.

According to Proposition 2, we can draw a conclusion that, for a specific pair of M and N , smaller values of \check{M} led to more unique and consecutive coarray lags. In other words, both numbers increase with the compression factor p . The minimum value that \check{M} can take is 1. In this case, the CACIS configuration becomes a nested array structure, which provides the highest numbers of the unique and consecutive virtual sensors. More detailed discussions about nested array configurations will be given in Section VI.

V. COPRIME ARRAY WITH DISPLACED SUBARRAYS

Sharing the same property as MRA, the prototype coprime array and the CACIS structure provide sparse configurations in which the minimum inter-element spacing remains the unit spacing, which is typically half wavelength, to avoid the grating lobe problem. In addition to the aforementioned challenges associated with half wavelength minimum spacing in regards of antenna size and mutual coupling, there is a high number of overlapping between the self- and cross-lags. This is the case

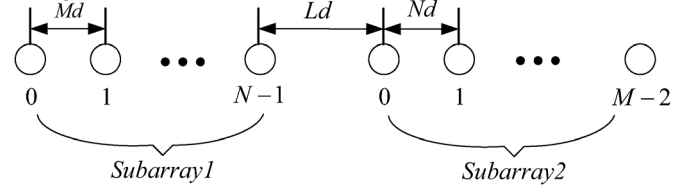


Fig. 5. The CADiS configuration.

for both the prototype coprime array and the CACIS structures and is consequence of the collocated subarray placement. By introducing a proper displacement between the two subarrays, the new coprime array structure achieves a larger minimum inter-element spacing, a higher number of unique lags, and a larger virtual array aperture. As we will see, however, the number of consecutive lags is reduced because the positive and negative lags are no longer connected.

Consider two collinearly located uniform linear subarrays, as depicted in Fig. 5, where one consists of N antennas and the other with $M - 1$ antennas. As such, the total number of the sensors is kept to $M + N - 1$. We refer to this coprime array structure as coprime array with displaced subarrays (CADiS). Similar to the CACIS configuration, we assume M and N are coprime. The N -element subarray has an inter-element spacing of $\check{M}d$, and the $(M - 1)$ -element subarray has an inter-element spacing of Nd , where, as indicated in (17), $M = p\check{M}$. The difference to the CASIS structure lies in the fact that these two subarrays in the CADiS structure are placed collinearly with the closest spacing between the two subarrays set to Ld , where $L \geq \min\{\check{M}, N\}$. Note that $\check{M} > 1$ is required to guarantee the minimum inter-element spacing to be larger than unit spacing, but the nested structure under this configuration, i.e., $\check{M} = 1$, will also be discussed later as a special case. The total number of array sensors in the CADiS structure remains $M + N - 1$, which is the same as the CACIS configuration discussed earlier. Note that the minimum inter-element spacing in the CADiS is $\min\{\check{M}, N\}d$, as compared to d in the CACIS structure. In addition, the total array aperture of the CADiS is $(MN + \check{M}N - \check{M} - 2N + L)d$, which is much larger than the $(M - 1)Nd$ of the CACIS. In practical application, however, a small value of displacement L should be chosen to avoid false peaks.

For the CADiS configuration, the corresponding self-lags $\check{\mathbb{L}}_s$ and cross-lags $\check{\mathbb{L}}_c$ are respectively given by²

$$\check{\mathbb{L}}_s = \{\check{l}_s | \check{l}_s = Nm\} \cup \{\check{l}_s | \check{l}_s = \check{M}n\}, \quad (20)$$

$$\check{\mathbb{L}}_c = \{\check{l}_c | \check{l}_c = \check{M}(N - 1) + Nm - \check{M}n + L\}, \quad (21)$$

²($\bar{\cdot}$) is used to emphasize variables corresponding to the CADiS structure.



Fig. 6. An example of CADiS configuration coarrays, where $p = 2$, $\check{M} = 3$, $N = 7$ and $L = \check{M} + N$.

TABLE I
COMPARISON OF THE COARRAY APERTURE, NUMBER OF UNIQUE LAGS, AND NUMBER OF CONSECUTIVE LAGS

	Coarray aperture	Maximum number of unique lags	Maximum number of consecutive lags
CACIS	$(M - 1)N$	$2MN - \check{M}(N - 1) - N$	$2MN - 2\check{M}(N - 1) - 1$
CADiS ($\check{M} > 1$) (displacement L)	$(N - 1)\check{M} + (M - 2)N + L$ (arbitrary L)	$2MN + 2M - 5$ ($L > N(M - 2)$)	$MN - (\check{M} - 1)(N - 2) + 1$ ($L = \check{M} + N$)
Nested CADiS ($\check{M} = 1$) (displacement L)	MN ($L = N + 1$)	$2MN + 1$ ($L = N + 1$)	$2MN + 1$ ($L = N + 1$)

and their corresponding mirrored positions $\bar{\mathbb{L}}_s^-$ and $\bar{\mathbb{L}}_c^-$, respectively, where $0 \leq m \leq M - 2$ and $0 \leq n \leq N - 1$.

The following proposition reveals the properties of the resulting virtual sensors of the CADiS configuration.

Proposition 3: Set $\bar{\mathbb{L}}_s$ and $\bar{\mathbb{L}}_c$ have the following properties in the CADiS configuration:

- There are $(M - 1)N$ distinct integers in set $\bar{\mathbb{L}}_c$.
- $\bar{\mathbb{L}}_c$ contains all the contiguous integers in the range $(\check{M} - 1)(N - 1) + L \leq \bar{l}_c \leq MN - N - 1 + L$.
- There are ‘‘holes’’ located at $\check{M}(N - 1) - (a\check{M} + bN) + L$ in set $\bar{\mathbb{L}}_c$, where $a \geq 0$, $b > 0$ are integers.
- $(\bar{\mathbb{L}}_s^- \cup \bar{\mathbb{L}}_s) \not\subseteq (\bar{\mathbb{L}}_c^- \cup \bar{\mathbb{L}}_c)$.

The proof is provided in Appendix III.

In the CACIS configuration, the negative lags form a subset of the flipped positive counterpart. Therefore, only non-negative lags in $\bar{\mathbb{L}}_c$ are used. In the CADiS configuration, however, the negative lags do not generally overlap with the flipped positive lags because of the displacement between two subarrays, necessitating the consideration of both positive and negative lags. As such, the CADiS configuration enjoys a higher number of unique lags than the CACIS because of the utilization of negative lags. In addition, the self-lags are less likely to coincide with the cross-lags in the CADiS configuration. Consequently, the CADiS offers a larger virtual array aperture and a higher number of virtual sensors. The role of the displacement L is as follows. On one hand, it reduces the overlaps between the self- and cross-lags. On the other hand, because $\bar{\mathbb{L}}_c$ has holes located at $\check{M}(N - 1) - (a\check{M} + bN) + L$ for integers $a \geq 0$ and $b > 0$, the number of consecutive lags can be extended by choosing an approximate value of L so that some self-lags are aligned to the cross-lag holes. For illustrative purpose, we consider the case of $p = 2$, $\check{M} = 3$, $N = 7$ and $L = \check{M} + N$ as an example. The corresponding $\bar{\mathbb{L}}_s$ and $\bar{\mathbb{L}}_c$ are shown in Fig. 6. It is clear that some holes in $\bar{\mathbb{L}}_c$ (12, 14, 15, 18 and 21) are aligned by elements of $\bar{\mathbb{L}}_s$. The following proposition describes the selection of the value of L that maximizes the number of unique and consecutive lags.

Proposition 4: For the CADiS configuration,

- The maximum number of unique lags $2MN + 2M - 5$ can be achieved with $L > N(M - 2)$.

- $L = \check{M} + N$ is the choice that yields the largest number of consecutive lags. In this case, there are $2MN + 2\check{M} - 1$ unique lags, among which the range $[(\check{M} - 1)(N - 1), MN + \check{M} - 1]$ and its corresponding negative range $[-MN - \check{M} + 1, -(\check{M} - 1)(N - 1)]$ are respectively consecutive.

The proof is provided in Appendix IV. Based on property (2) of Proposition 4, it is clear that the number of unique lags increases as \check{M} increases, whereas the number of the consecutive lags decreases. Particularly, for the nested array structure, i.e., $\check{M} = 1$, the positive range of consecutive lags is $[0, MN]$ and its corresponding negative range becomes $[-MN, 0]$, resulting in all unique lags to be consecutive.

For comparison, we enlist in Table I the coarray aperture, the maximum number of unique and consecutive lags for both proposed configurations. As the results show, for a given coprime pair of M and N , the nested structure achieves the maximum number of consecutive and unique lags when using CACIS configurations. In other word, it offers the highest number of DOFs for DOA estimation. As for CADiS, the nested structure provides the highest number only for the consecutive lags. The number of its unique lags, $2MN + 1$, on the other hand, is less than that of the CADiS structure with a large separation between the two subarrays. That is, the nested CADiS provides the highest number of DOFs only when MUSIC or other subspace based methods are used for DOA estimation, but it becomes less effective when CS based DOA estimation methods are applied. It is noted that, to estimate DOAs of up to MN sources, the nested CADiS structure requires only $M + N - 1$ sensors, which are much less than the result of $2M + N - 1$ sensors as exploited in [13].

VI. COMPARISON OF DIFFERENT NESTED STRUCTURES

The nested structure is referred to a structure consisting of two uniform linear subarrays, where one subarray has a unit inter-element spacing [9]. A nested array is usually designed such that the virtual sensors in the resulting coarray are all contiguous. The nested structure proposed in [9], as shown in Fig. 7, consists of an inner N_1 -element subarray with a unit spacing d

TABLE II
 OPTIMUM SOLUTION FOR DIFFERENT NESTED STRUCTURES THAT MAXIMIZES THE DOFS

The number of physical sensors			Optimal values	Maximum number of DOFs
CACIS	$K = M + N - 1$	K is even	$M = \frac{K+2}{2}, N = \frac{K}{2}$	$(M-1)N = \frac{K^2}{4}$
		K is odd	$M = \frac{K+1}{2}, N = \frac{K+1}{2}$	$(M-1)N = \frac{K^2-1}{4}$
CADiS	$K = M + N - 1$	K is even	$M = \frac{K+2}{2}, N = \frac{K}{2}$	$MN = \frac{K^2+2K}{4}$
		K is odd	$M = \frac{K+1}{2}, N = \frac{K+1}{2}$	$MN = \frac{K^2+2K+1}{4}$
Configuration in [9]	$K = N_1 + N_2$	K is even	$N_1 = \frac{K}{2}, N_2 = \frac{K}{2}$	$N_2(N_1+1) - 1 = \frac{K^2+2K-4}{4}$
		K is odd	$N_1 = \frac{K-1}{2}, N_2 = \frac{K+1}{2}$	$N_2(N_1+1) - 1 = \frac{K^2+2K-3}{4}$

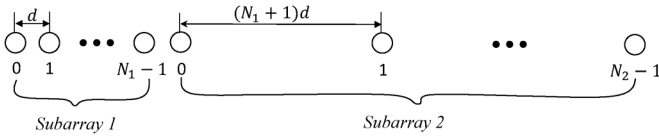
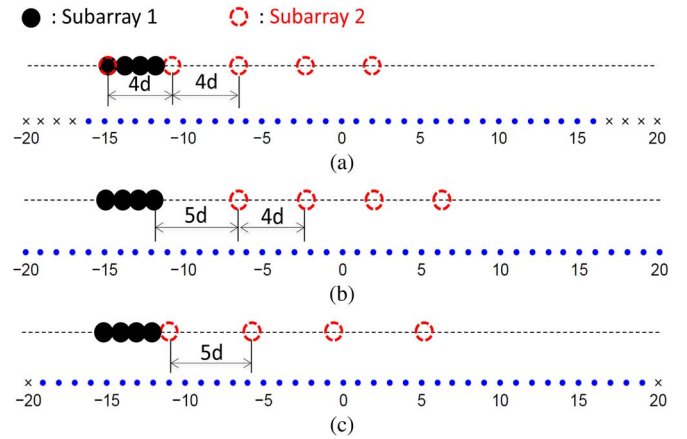


Fig. 7. The nested configuration proposed in [9].

and an outer N_2 -element subarray with spacing $(N_1 + 1)d$, resulting in $2N_2(N_1 + 1) - 1$ contiguous lags. Note that the nested array concept does not require a coprimality between N_1 and N_2 . It is also important to note that, in the extension of the generalized coprime array framework, different nested array configurations can be defined, by setting \tilde{M} to be one to the CACIS and CADiS structures. These different nested configurations yield different numbers of DOFs. For comparison of the three nested array structures, we consider the same number, K , of physical sensors, and optimize the array configuration for each structure to maximize the respective number of DOFs. Such optimal solutions are summarized in Table II. It is clear that the structure in [9] offers a higher number of DOFs than the nested CACIS structure, but less than the nested CADiS.

For better illustrative purposes, we compare three different optimized nested configurations with $K = 8$ physical sensors in Fig. 8. Fig. 8(a) shows the optimized nested CACIS configuration. One subarray is of $N = 4$ sensors with an inter-element spacing of $\tilde{M}d = d$, whereas the other is of $M = 5$ elements with an inter-element spacing of $Nd = 4d$. In addition, the two subarrays share the first sensor at the zeroth position and form a coarray with 33 lag positions. The nested CADiS structure is illustrated in Fig. 8(b). One 4-element subarray has an inter-element spacing of $\tilde{M}d = d$, and the other subarray has an inter-element spacing of $Nd = 4d$. In addition, there is a displacement $Ld = (\tilde{M} + N)d = 5d$ between the two subarrays. As a result, its coarray has 41 lag positions. Finally, the nested array configuration proposed in [9] is depicted in Fig. 8(c), where the inner subarray has $N_1 = 4$ elements with spacing d and the outer subarray has $N_2 = 4$ elements with spacing $(N_1 + 1)d = 5d$. In


 Fig. 8. Three different optimized nested configurations and their coarrays ($K = 8$). (a) The nested CACIS. (b) The nested CADiS. (c) The nested configuration proposed in [9].

this case, the coarray has 39 lag positions. As a result, the nested CADiS structure achieves a higher number of DOFs.

VII. SIMULATION RESULTS

For illustrative purposes, we consider $M = 6$ and $N = 7$ with different values of the compression factor p of the two configurations, i.e., CACIS and CADiS. $L = \tilde{M} + N$ are considered for the CADiS configuration for the convenience of performance comparison between both MUSIC and CS techniques. All configurations consist of $M + N - 1 = 12$ physical antenna sensors and the unit inter-element spacing is $d = \lambda/2$.

A. Array Configurations

The virtual sensors corresponding to the CACIS and CADiS structures are respectively shown in Fig. 9 and Fig. 10. Fig. 9(a) depicts the CACIS configuration example for $p = 2$, where the coprime array form a virtual array with 59 unique lags, among which 47 lags within $[-23, 23]$ are consecutive. Fig. 9(b) shows for the case of $p = 3$, and the resulting virtual array has 65

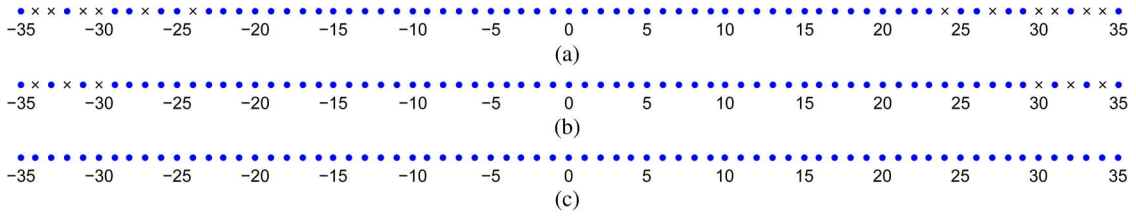


Fig. 9. CACIS configuration coarrays, for different compression factor p ($M = 6$ and $N = 7$). (a) $p = 2$ and $\tilde{M} = 3$. (b) $p = 3$ and $\tilde{M} = 2$. (c) $p = 6$ and $\tilde{M} = 1$.

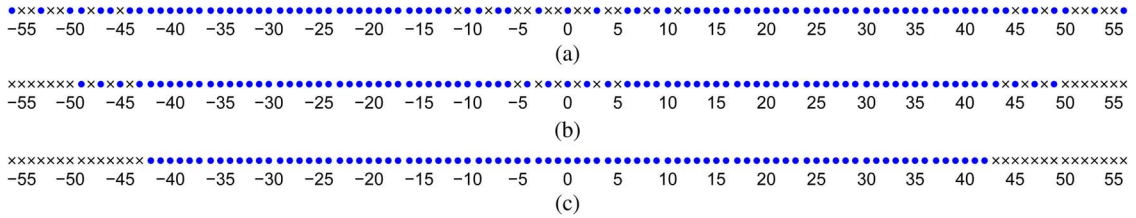


Fig. 10. CADiS configuration coarrays with displacement $L = \tilde{M} + N$, corresponding the compression factor p ($M = 6$ and $N = 7$). (a) $p = 2$, $\tilde{M} = 3$ and $L = 10$. (b) $p = 3$, $\tilde{M} = 2$ and $L = 9$. (c) $p = 6$, $\tilde{M} = 1$ and $L = 8$.

unique lags, among which 59 lags within $[-29, 29]$ are consecutive. When $p = M = 6$, i.e., $\tilde{M} = 1$, as shown in Fig. 9(c), the coprime array becomes the nested array structure with 71 unique lags, which are all consecutive. It is clear that both numbers of the unique and consecutive lags increase with p , and the nested array achieves the maximum number for both. For the CADiS configuration with $L = \tilde{M} + N$, the case of $p = 2$ is presented in Fig. 10(a). In this case, the entire virtual array has 89 unique lags, among which lags within $[-44, -12]$ and $[12, 44]$ are respectively consecutive. For $p = 3$, there are 87 distinct lags, resulting consecutive lags in $[-43, -6]$ and in $[6, 43]$ as shown in Fig. 10(b). In Fig. 10(c), the nested CADiS with $p = 6$ and $\tilde{M} = 1$ is considered as a special case. It is noted that all 85 lags in the full symmetric set of $[-42, 42]$ are consecutive.

B. MUSIC and CS Spectra

In Figs. 11 and 12, we present numerical examples to demonstrate the number of achievable DOFs for DOA estimation using the generalized coprime arrays. As the virtual sensor lags are obtained from the estimated covariance matrix based on the received data samples as in (5), the virtual steering matrix is sensitive to the noise contamination. To clearly demonstrate the number of achievable DOFs, therefore, we use 2000 noise-free snapshots to obtain a relatively clean covariance matrix. $Q = 33$ uncorrelated narrowband sources are considered, which are uniformly distributed between -60° and 60° . For the MUSIC algorithm which requires consecutive lags, we respectively obtain 23, 29 and 35 DOFs of CACIS configuration for $p = 2$, $p = 3$ and $p = 6$ as shown in Figs. 11(a), 11(c) and 11(e). On the other hand, 17, 19 and 42 DOFs are obtained using the CADiS configuration as shown in Figs. 11(b), 11(d) and 11(f). Note that only the nested structures have a sufficient number of DOFs to resolve all 33 impinging signals. This is verified in Fig. 11 in which only the cases of $p = 6$ resolve all the 33 signals for both configurations, whereas not all sources are correctly identified for the cases of $p = 2$ and $p = 3$. In addition, it is evident that the “nested CADiS” has better performance than “nested CACIS” due to the higher DOFs of the former. When the CS technique is applied for DOA estimation, a higher number of

DOFs is achieved because all unique lags are exploited. The results obtained from the Lasso are shown in Fig. 12, where a grid interval of $\theta_i^g = 0.25^\circ$ and the penalty parameter of $\lambda_t = 0.85$ are used. It is clearly shown that only the nested structure can recover all 33 sources using the CACIS configuration, whereas all these signals can be detected for all the CADiS configurations examined in Fig. 12 due to their higher unique lags. In addition, the CS based technique results in better estimated spectra, when comparing the MUSIC spectra depicted in Fig. 11.

To compare the performance between the CACIS and CADiS structures as well as between the MUSIC and CS methods, we use the respective nested structures and compute the results in the presence of noise with a 0 dB SNR for all signals, and the number of snapshots is reduced to 500. In this case, the perturbation in the covariance matrix becomes higher due to noise and the limited number of samples, and the resulting DOA estimation performance degrades. The DOA estimation results are compared in Fig. 13 for $Q = 33$ sources, which is smaller than the available DOFs for both array configurations. It is evident that the nested CADiS outperforms the nested CACIS, and the CS based method achieves a better spatial spectrum estimation performance.

C. Root Mean Square Error Versus SNR and Number of Snapshots

We further compare the DOA estimation performance of different CACIS and CADiS configurations through Monte Carlo simulations. The average root mean square error (RMSE) of the estimated DOAs, expressed as

$$\text{RMSE} = \sqrt{\frac{\sum_{i=1}^I \sum_{q=1}^Q (\hat{\theta}_q(i) - \theta_q)^2}{IQ}},$$

is used as the performance metric, where $\hat{\theta}_q(i)$ is the estimate of θ_q for the i th Monte Carlo trial, $i = 1, \dots, I$. We use $I = 500$ independent trials in all simulations.

To enable comparison, we consider $Q = 16$ narrowband uncorrelated sources, which are lower than the available DOFs for

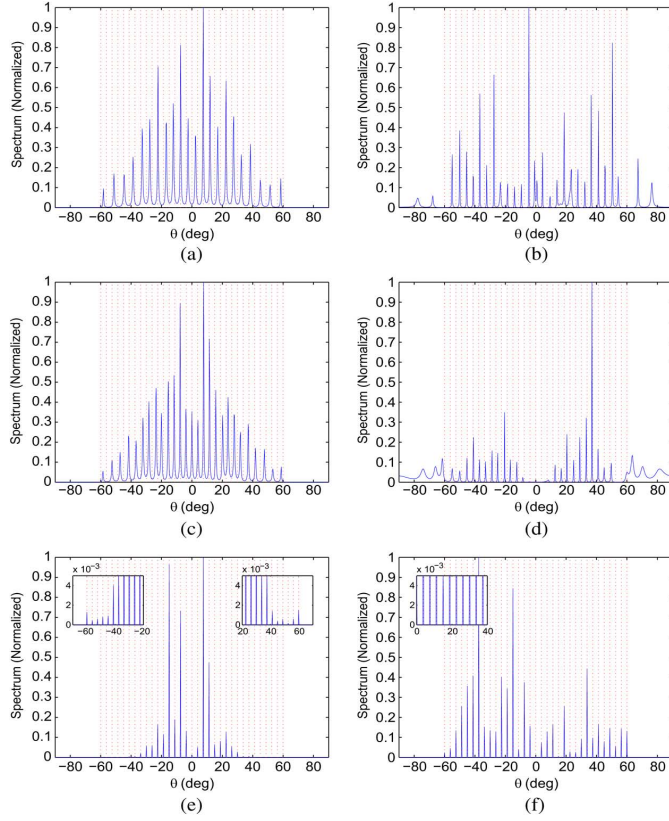


Fig. 11. Spatial spectra estimated using MUSIC for both configurations ($Q = 33$, $M = 6$ and $N = 7$). (a) CACIS with $p = 2$. (b) CADiS with $p = 2$. (c) CACIS with $p = 3$. (d) CADiS with $p = 3$. (e) CACIS with $p = 6$. (f) CADiS with $p = 6$.

all cases with both MUSIC and CS techniques. Fig. 14 compares the RMSE performance as a function of the input SNR, where 500 snapshots are used. In Fig. 15, we compare the performance of different array configurations and DOA techniques with respect to the number of snapshots, where the input SNR is set to 0 dB. It is evident that the DOA estimation performance is improved with the increase of the input SNR and the number of snapshots. For the CACIS structure, the performance of both MUSIC and CS approaches improves as the compression factor p increases because of the increased number of consecutive and unique lags. As a result, the nested array structure achieves the best performance. For CADiS, MUSIC-based DOA estimation for non-nested CADiS structures suffers from significant performance degradation because of the disconnected coarray lags. As such, the nested array is the preferred CADiS structure when the MUSIC algorithm is used for DOA estimation. Furthermore, the nested CADiS slightly outperforms the nested CACIS as a result of higher number of consecutive lags. However, because it has the fewest unique lags, the nested structure is least effective among the three CADiS array structures when the CS technique is exploited. As a conclusion, the CS-based method obtains better performance than the MUSIC counterparts. In addition, when the CS-based technique is used, the CADiS outperforms the corresponding CACIS structures.

VIII. CONCLUSIONS

We have proposed the generalized coprime array concept in two aspects: compression of the inter-element of spacing of one

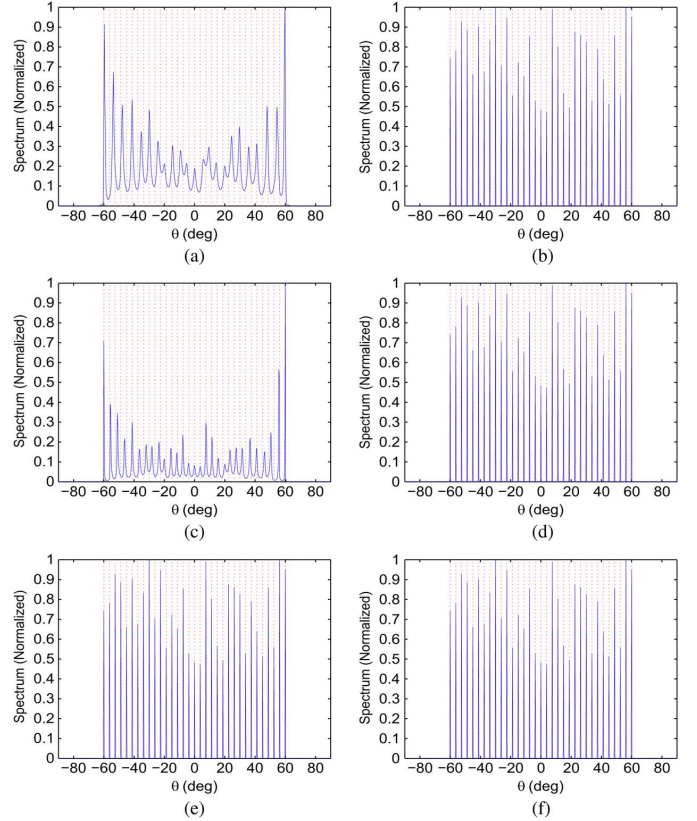


Fig. 12. Spatial spectra estimated using Lasso for both configurations ($Q = 33$, $M = 6$ and $N = 7$). (a) CACIS with $p = 2$. (b) CADiS with $p = 2$. (c) CACIS with $p = 3$. (d) CADiS with $p = 3$. (e) CACIS with $p = 6$. (f) CADiS with $p = 6$.

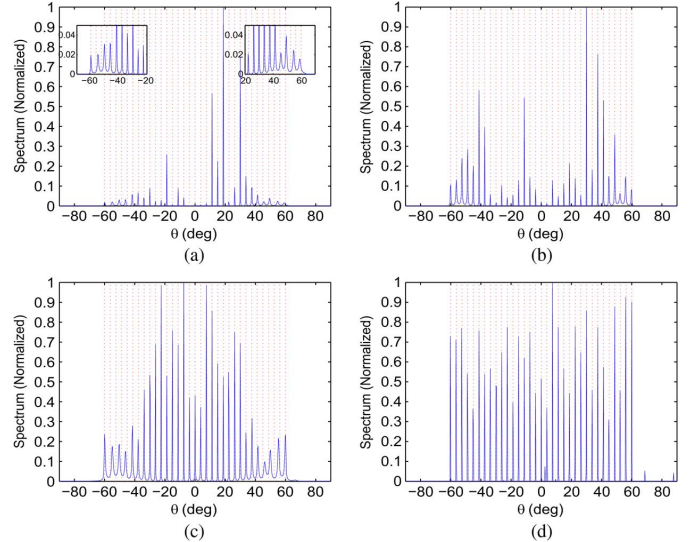
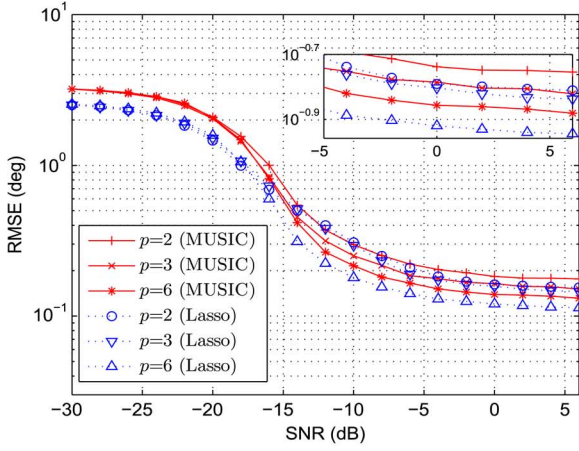
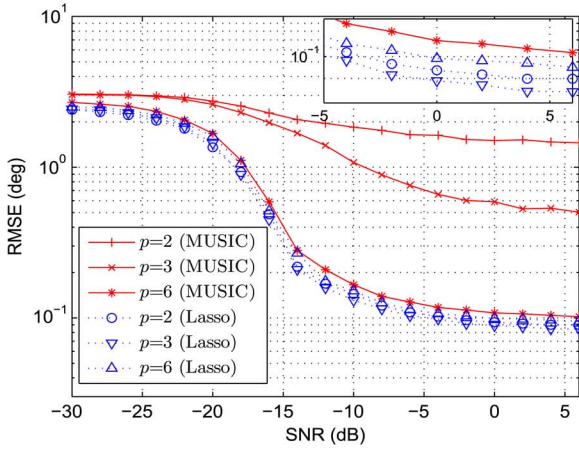


Fig. 13. Estimated spatial spectra (SNR = 0 dB, 500 snapshots, $Q = 33$). (a) MUSIC with nested CACIS. (b) MUSIC with nested CADiS. (c) LASSO with nested CADiS. (d) LASSO with nested CADiS.

constituting subarray, and the displacement of the two subarrays. The first operation yields flexibility of trading-off between unique lags and consecutive lags for effective direction-of-arrival (DOA) estimation based on different algorithms, whereas the second operation further allows a larger minimum inter-element spacing beyond the typical half-wavelength requirement.



(a)



(b)

Fig. 14. RMSE versus SNR (500 snapshots, $Q = 16$). (a) The CACIS configurations. (b) The CADiS configurations.

The performance of the generalized coarray structures was evaluated using their difference coarray equivalence, and the analytical expressions of the coarray aperture, the achievable number of unique lags, and the maximum number of consecutive lags were derived for quantitative evaluation, comparison, and optimal design. The usefulness of these results was demonstrated using examples applied for DOA estimations.

APPENDIX I PROOF OF PROPOSITION 1

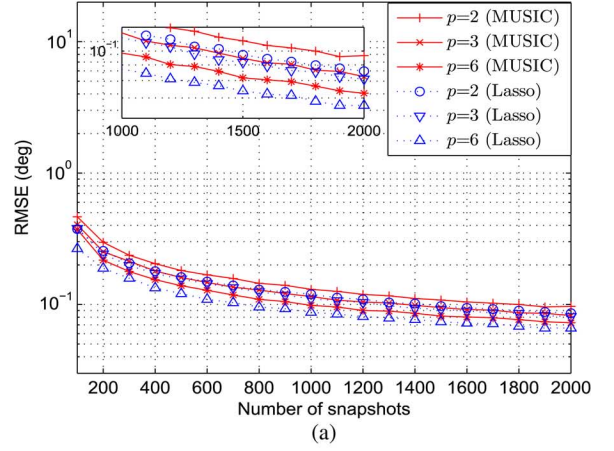
- (a) We prove it using contradiction. Denote $\tilde{l}_{c_1} = Nm_1 - \check{M}n_1$ and $\tilde{l}_{c_2} = Nm_2 - \check{M}n_2$ as two arbitrary lags in set \mathbb{L}_c , where $0 \leq m_1 \leq M-1$, $0 \leq m_2 \leq M-1$, $0 \leq n_1 \leq N-1$ and $0 \leq n_2 \leq N-1$. Had $\tilde{l}_{c_1} = \tilde{l}_{c_2}$ been held, we would have

$$\frac{\check{M}}{N} = \frac{m_1 - m_2}{n_1 - n_2}. \quad (22)$$

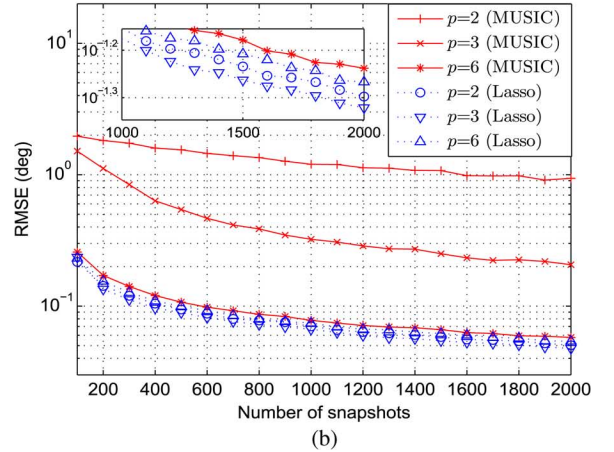
Since $n_1 - n_2 < N$, (22) cannot be hold due to the coprimality of \check{M} and N . That is, \tilde{l}_{c_1} and \tilde{l}_{c_2} cannot be equal. Thus, \mathbb{L}_c has MN distinct integers.

- (b) Given an arbitrary integer \tilde{l}_c in set \mathbb{L}_c satisfying

$$-(N-1) \leq \tilde{l}_c \leq MN - \check{M}(N-1) - 1, \quad (23)$$



(a)



(b)

Fig. 15. RMSE versus the number of snapshots (SNR = 0 dB, $Q = 16$). (a) The CACIS configurations. (b) The CADiS configurations.

we need to prove that there exist integers $m \in [0, M-1]$ and $n \in [0, N-1]$ such that $\tilde{l}_c = Nm - \check{M}n$ holds. The requirement $n \in [0, N-1]$ is equivalent to

$$0 \leq \check{M}n \leq \check{M}(N-1). \quad (24)$$

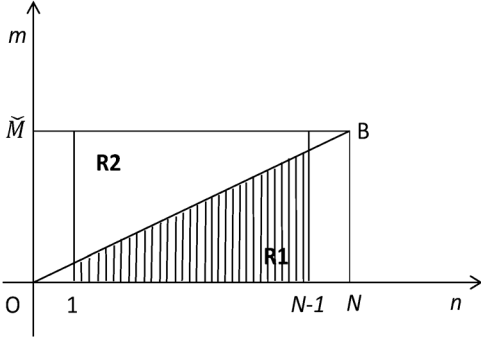
Because $Nm = \tilde{l}_c + \check{M}n$, we obtain the following relationship by combining (23) and (24),

$$-(N-1) \leq Nm \leq MN - 1. \quad (25)$$

This result can be equivalently expressed as $-N < Nm < MN$, which implies $-1 < m < M$. Because m is an integer, this requirement is equivalent to

$$0 \leq m \leq M-1, \quad (26)$$

which is satisfied in the underlying coprime array.
Remark: The configuration proposed in [13] becomes a special case of CACIS configuration, as $M = 2\check{M}$. As a result, the set \mathbb{L}_c contains all the integers in the range $-(N-1) \leq \tilde{l}_c \leq \check{M}N + \check{M} - 1$. Apparently, our result contains more consecutive lags and more precise than the results provided in [13] using the same configuration. In [13], they only count the consecutive \tilde{l}_c in the range $[0, \check{M}N]$.


 Fig. 16. The geometry of m and n .

- (c) Given an arbitrary integer in set $\tilde{\mathbb{L}}_c$ satisfying $\tilde{l}_c = Nm - \check{M}n < 0$, where $m \in [0, \check{M} - 1]$ and $n \in [0, N - 1]$, the following relationship can be obtained

$$0 \leq Nm < \check{M}n \leq \check{M}(N - 1) < \check{M}N. \quad (27)$$

Consequently, the set $\tilde{\mathbb{L}}_{c-}$, which consists of the negative elements in $\tilde{\mathbb{L}}_c$, can be expressed as

$$\tilde{\mathbb{L}}_{c-} = \{\tilde{l}_c | \tilde{l}_c = Nm - \check{M}n, Nm < \check{M}n\}, \quad (28)$$

where $0 \leq m \leq \check{M} - 1$ and $0 < n \leq N - 1$. Considering an arbitrary integer $\tilde{l}_{c_1} = Nm_1 - \check{M}n_1$ in set $\tilde{\mathbb{L}}_{c-}$, where $Nm_1 < \check{M}n_1$, $m_1 \in [0, \check{M} - 1]$ and $n_1 \in [0, N - 1]$, then we need to prove that there always exists \tilde{l}_{c_2} in set $\tilde{\mathbb{L}}_c$ to satisfy

$$\tilde{l}_{c_2} = Nm_2 - \check{M}n_2 = -\tilde{l}_{c_1} = \check{M}n_1 - Nm_1, \quad (29)$$

where integers $m_2 \in [0, \check{M} - 1]$ and $n_2 \in [0, N - 1]$. Then the relationship

$$\frac{\check{M}}{N} = \frac{m_1 + m_2}{n_1 + n_2}, \quad (30)$$

must be valid. Since $n_1 + n_2 \in (0, 2N)$ and \check{M} and N are coprime, it is indicated that \check{M}/N cannot be reduced to a ratio of smaller integers. As a result, the requirement is equivalent to

$$\begin{aligned} m_2 &= \check{M} - m_1, \\ n_2 &= N - n_1, \end{aligned} \quad (31)$$

It is clear that there always exists $m_2 \in [1, \check{M}] \subseteq [0, \check{M} - 1]$ and $n_2 \in [0, N - 1]$ to satisfy (31).

- (d) Because the two subarrays share the first sensor at the zeroth position, the self-lags can be taken as cross-lags between every sensor of one subarray and the first sensor of the other subarray. Thus, $(\tilde{\mathbb{L}}_s^- \cup \tilde{\mathbb{L}}_s) \subseteq (\tilde{\mathbb{L}}_c^- \cup \tilde{\mathbb{L}}_c)$.
- (e) We prove the proposition by contradiction. Based on (28), we suppose $Nm - \check{M}n = -(a\check{M} + bN)$ holds for some integers $m \in (0, \check{M})$ and $n \in (0, N)$, where $a \geq 0$ and $b > 0$ are integers, then relationship

$$\frac{\check{M}}{N} = \frac{m + b}{n - a} \quad (32)$$

must be valid. From $0 < n < N$ and $a \geq 0$, we find $n - a < N$. As such, due to the coprimality between \check{M}

and N , we cannot find an integer m that satisfies (32). Therefore, $Nm - \check{M}n \neq -(a\check{M} + bN)$, i.e., there are holes at $-(a\check{M} + bN)$ in set $\tilde{\mathbb{L}}_c$.

APPENDIX II PROOF OF PROPOSITION 2

- (a) In line with the property (d) of Proposition 1, the full symmetric set of lags which defined in (10) can be expressed as

$$\tilde{\mathbb{L}}_P = \tilde{\mathbb{L}}_c^- \cup \tilde{\mathbb{L}}_c. \quad (33)$$

Because $\tilde{\mathbb{L}}_c$ can be denoted as

$$\tilde{\mathbb{L}}_c = \{\tilde{l}_c | \tilde{l}_c \geq 0, \tilde{l}_c \in \tilde{\mathbb{L}}_c\} \cup \{\tilde{l}_c | \tilde{l}_c < 0, \tilde{l}_c \in \tilde{\mathbb{L}}_c\}, \quad (34)$$

(33) is equivalent to

$$\tilde{\mathbb{L}}_P = \{\pm\tilde{l}_c | \tilde{l}_c \geq 0, \tilde{l}_c \in \tilde{\mathbb{L}}_c\} \cup \{\pm\tilde{l}_c | \tilde{l}_c < 0, \tilde{l}_c \in \tilde{\mathbb{L}}_c\}. \quad (35)$$

Based on the property (c) of Proposition 1, the negative values form a subset of the flipped positive values in set $\tilde{\mathbb{L}}_c$. It is indicated that $\{\tilde{l}_c | \tilde{l}_c < 0, \tilde{l}_c \in \tilde{\mathbb{L}}_c\} \subseteq \{-\tilde{l}_c | \tilde{l}_c > 0, \tilde{l}_c \in \tilde{\mathbb{L}}_c\}$ and $\{-\tilde{l}_c | \tilde{l}_c < 0, \tilde{l}_c \in \tilde{\mathbb{L}}_c\} \subseteq \{\tilde{l}_c | \tilde{l}_c > 0, \tilde{l}_c \in \tilde{\mathbb{L}}_c\}$. Finally, the set $\tilde{\mathbb{L}}_P$ becomes

$$\tilde{\mathbb{L}}_P = \{\tilde{l}_c | \tilde{l}_c \geq 0, \tilde{l}_c \in \tilde{\mathbb{L}}_c\} \cup \{-\tilde{l}_c | \tilde{l}_c \geq 0, \tilde{l}_c \in \tilde{\mathbb{L}}_c\}, \quad (36)$$

Denote $\tilde{\eta}_c$ and $\tilde{\eta}_{c-}$ as the number of distinct lags in set $\tilde{\mathbb{L}}_c$ and $\tilde{\mathbb{L}}_{c-}$, respectively. As a result of (36), the number of distinct lags in set $\tilde{\mathbb{L}}_P$ can be expressed as

$$\tilde{\eta}_P = 2(\tilde{\eta}_c - \tilde{\eta}_{c-}) - 1, \quad (37)$$

where $\tilde{\eta}_c - \tilde{\eta}_{c-}$ represents the number of non-negative lags in set $\tilde{\mathbb{L}}_c$. Due to the property (a) of Proposition 1, there are MN distinct integers in set $\tilde{\mathbb{L}}_c$. It is easy to confirm that

$$\tilde{\eta}_c = MN. \quad (38)$$

$\tilde{\eta}_P$ can be obtained easily if given $\tilde{\eta}_{c-}$. Next, the derivation of $\tilde{\eta}_{c-}$ is given as follows. According to the definition of $\tilde{\mathbb{L}}_{c-}$ defined in (28),

$$\tilde{\mathbb{L}}_{c-} = \{\tilde{l}_c | \tilde{l}_c = Nm - \check{M}n, Nm < \check{M}n\},$$

where $0 \leq m \leq \check{M} - 1$ and $0 < n \leq N - 1$. For illustration, the geometry distribution of m and n , is shown in Fig. 16. As such, the boundary and interior of the shadow part **R1** represents all elements in $\tilde{\mathbb{L}}_{c-}$. Since \check{M} and N are coprime, there is no integer point on the diagonal line between OB . In addition, the shadow part **R1** is symmetric with **R2**. As a consequence, for obtaining the number of elements in set $\tilde{\mathbb{L}}_{c-}$, we can first calculate the number of integer points in the rectangle within $[0, \check{M}]$ and $[1, N - 1]$ and then get the half of that number. There are $(\check{M} + 1)$ and $(N - 1)$ integers in the range $[0, \check{M}]$ and $[1, N - 1]$, respectively, thus, we obtain

$$\tilde{\eta}_{c-} = \frac{(\check{M} + 1)(N - 1)}{2}, \quad (39)$$

Finally, substituting (38) and (39) into (37),

$$\tilde{\eta}_P = 2MN - (\check{M} + 1)(N - 1) - 1, \quad (40)$$

is derived analytically.

- (b) On the basis of property (b) of Proposition 1, $\bar{\mathbb{L}}_c$ contains all the contiguous integers in the range $-(N - 1) \leq \bar{l}_c \leq MN - \check{M}(N - 1) - 1$. Then, it is easy to confirm that $\bar{\mathbb{L}}_P$ contains $2MN - 2\check{M}(N - 1) - 1$ consecutive integers in the range $[-MN + \check{M}(N - 1) + 1, MN - \check{M}(N - 1) - 1]$ in terms of (36).

APPENDIX III PROOF OF PROPOSITION 3

- (a) The proof can be extended from the proof of property (a) of Proposition 1, i.e., two arbitrary lags \bar{l}_{c_1} and \bar{l}_{c_2} in set $\bar{\mathbb{L}}_c$ cannot be equal. Thus, $\bar{\mathbb{L}}_c$ has $(M - 1)N$ distinct integers.
- (b) The set $\bar{\mathbb{L}}_c$ can be rewritten as

$$\bar{\mathbb{L}}_c = \left\{ \bar{l}_c \mid \bar{l}_c = \check{M}(N - 1) + z + L \right\}, \quad (41)$$

where $0 \leq m \leq M - 2$ and $0 \leq n \leq N - 1$, for different values of z that falls into the following set,

$$\mathbb{Z} = \{z \mid z = Nm - \check{M}n, 0 \leq m \leq M - 2, 0 \leq n \leq N - 1\}. \quad (42)$$

Extended from the proof of the property (b) of Proposition 1, we can conclude that z is consecutive in the range

$$-(N - 1) \leq z \leq MN - \check{M}(N - 1) - N - 1. \quad (43)$$

Combining (41) and (43), $\bar{\mathbb{L}}_c$ contains all the contiguous integers in the range

$$(\check{M} - 1)(N - 1) + L \leq \bar{l}_c \leq MN - N - 1 + L. \quad (44)$$

- (c) Based on the proof of property (e) of Proposition 1, it is easy to confirm that there are some holes located at $-(a\check{M} + bN)$ in the negative range of set \mathbb{Z} , where $a \geq 0, b > 0$ are integers. Then we can draw a conclusion that there are holes located at $\check{M}(N - 1) - (a\check{M} + bN) + L$ in set $\bar{\mathbb{L}}_c$ by combining (41) and (42).
- (d) Due to the displacement, the two subarray do not share the first sensor any more. Considering the elements in set $\bar{\mathbb{L}}_s, 0 \notin \bar{\mathbb{L}}_c$ because the minimum value in $\bar{\mathbb{L}}_c$ is L , which is larger than 1. Consequently, $(\bar{\mathbb{L}}_s^- \cup \bar{\mathbb{L}}_s) \not\subseteq (\bar{\mathbb{L}}_c^- \cup \bar{\mathbb{L}}_c)$.

APPENDIX IV PROOF OF PROPOSITION 4

- (a) Denote $\bar{\eta}_s$ and $\bar{\eta}_c$ as the number of the distinct lags in sets $\bar{\mathbb{L}}_s$ and $\bar{\mathbb{L}}_c$, respectively, and $\bar{\eta}_o$ as the number of overlaps between the $\bar{\mathbb{L}}_s$ and $\bar{\mathbb{L}}_c$. Based on the definition of $\bar{\mathbb{L}}_P$ and $\bar{\mathbb{L}}_s$ in (21), all lags in these sets are positive. As a consequence of this, the number of full symmetric set of lags in the virtual array can be expressed as

$$\bar{\eta}_P = 2(\bar{\eta}_s + \bar{\eta}_c - \bar{\eta}_o) - 1. \quad (45)$$

Because of the coprimality of \check{M} and N , $\check{M}n \neq Nm$ for $n \in (0, N - 1]$ and $m \in (0, M - 2]$. As such,

$$\bar{\eta}_s = M + N - 2. \quad (46)$$

In line with the property (a) of Proposition 1, we can obtain

$$\bar{\eta}_c = (M - 1)N. \quad (47)$$

Substituting (46) and (47) into (45), the relationship is equivalent to

$$\bar{\eta}_P = 2(MN + M - 2 - \bar{\eta}_o) - 1. \quad (48)$$

When $L > N(M - 2)$, the maximum value in $\bar{\mathbb{L}}_s$ is less than the minimum value in $\bar{\mathbb{L}}_c$. It signifies that there is no overlap between $\bar{\mathbb{L}}_s$ and $\bar{\mathbb{L}}_c$, i.e., $\bar{\eta}_o = 0$. Then the maximum number of unique lags, which is $2MN + 2M - 5$, can be achieved.

- (b) Due to the coprimality of \check{M} and N , any integer value for displacement, L , can be realized by an appropriate choice of integers c_1 and c_2 , i.e., [30]

$$L = c_1\check{M} + c_2N. \quad (49)$$

Based on the property (c) of the Proposition 3, there are holes located at $\check{M}(N - 1) - (a\check{M} + bN) + L$ in set $\bar{\mathbb{L}}_c$, where with a and b are integers and $a \in [0, \infty), b \in (0, \infty)$. If some holes are aligned by the elements in $\bar{\mathbb{L}}_s$, the following relationship

$$\check{M}(N - 1) - (a\check{M} + bN) + L = Nm, \quad (50)$$

or

$$\check{M}(N - 1) - (a\check{M} + bN) + L = \check{M}n \quad (51)$$

must be valid. Substituting (49) into (50) and (51), the requirement is equivalent to

$$\check{M}N + (c_1 - a - 1)\check{M} + (c_2 - b)N = Nm,$$

or

$$\check{M}N + (c_1 - a - 1)\check{M} + (c_2 - b)N = \check{M}n,$$

i.e.,

$$c_1 = a + 1 \quad \text{or} \quad c_2 = b. \quad (52)$$

Then the requirement further becomes

$$c_1 = 1 \quad \text{or} \quad c_2 = 1, \quad (53)$$

so that the first hole ($a = 0$ and $b = 1$), which is outside the consecutive range of $\bar{\mathbb{L}}_c$, can be aligned. When $c_1 = 1$, i.e., $L = \check{M} + c_2N$, the holes, where $a = 0$ and arbitrary $b > 0$,

$$\begin{aligned} & \check{M}(N - 1) - bN + L \\ &= \check{M}(N - 1) - bN + \check{M} + c_2N \\ &= (\check{M} - b + c_2)N, \end{aligned} \quad (54)$$

When $c_2 = 1$, i.e., $L = c_1\check{M} + N$, the holes, where arbitrary $a \geq 0$ and $b = 1$,

$$\begin{aligned} & \check{M}(N-1) - (a\check{M} + N) + L \\ &= \check{M}(N-1) - (a\check{M} + N) + c_1\check{M} + N \\ &= (N-1-a+c_1)\check{M}, \end{aligned}$$

are aligned. Thus, $c_1 = c_2 = 1$, i.e., $L = \check{M} + N$, is the optimal choice since all above holes can be aligned. In this case, the holes, where $a = 0$ and $b = 1$, $a = 0$ and $b = 2$, $a = 1$ and $b = 1$, are aligned. As a result, the first hole outside the consecutive range of $\bar{\mathbb{L}}_c$ becomes $\check{M}(N-1) - (\check{M} + 2N) + L$ where $a = 1$ and $b = 2$. Then, the set $\bar{\mathbb{L}}_c$ contains all the consecutive integers in the range

$$\check{M}(N-1) - (\check{M} + 2N) + L \leq \bar{l}_c \leq MN - N - 1 + L, \quad (55)$$

where $L = \check{M} + N$. It is simplified as,

$$(\check{M}-1)(N-1) \leq \bar{l}_c \leq MN + \check{M} - 1. \quad (56)$$

Next, we give the proof of the number of the unique lags when $L = \check{M} + N$. The following relationship

$$\check{M}(N-1) + (Nm_1 - \check{M}n_1) + \check{M} + N = Nm_2, \quad (57)$$

or

$$\check{M}(N-1) + (Nm_1 - \check{M}n_1) + \check{M} + N = \check{M}n_2, \quad (58)$$

must be valid if $\bar{\mathbb{L}}_s$ overlaps with $\bar{\mathbb{L}}_c$. It is equivalent to

$$\check{M} + m_1 + 1 - n_1 \frac{\check{M}}{N} = m_2, \quad (59)$$

or

$$N - n_1 + (m_1 + 1) \frac{N}{\check{M}} = n_2. \quad (60)$$

In (59), n_1 must be equal to 0 because m_2 is an integer, yielding

$$\check{M} + m_1 + 1 = m_2. \quad (61)$$

It is clear to confirm $m_2 \in [0, M - \check{M} - 3]$ since $m_1 \in [0, M - 2]$. This suggests that the number of the overlaps in (59) is $M - \check{M} - 2$. Similarly, we can show the number of overlaps in (60) is 0. Hence,

$$\bar{\eta}_o = M - \check{M} - 2. \quad (62)$$

Substituting (62) into (48), we can obtain the number of unique lags $\bar{\eta}_P$ to be

$$\bar{\eta}_P = 2MN + 2\check{M} - 1. \quad (63)$$

ACKNOWLEDGMENT

The authors would like to thank the reviewers for the many constructive suggestions and comments.

REFERENCES

- [1] Y. D. Zhang, S. Qin, and M. G. Amin, "DOA estimation exploiting coprime arrays with sparse sensor spacing," in *Proc. IEEE ICASSP*, Florence, Italy, May 2014, pp. 2267–2271.
- [2] S. Qin, Y. D. Zhang, and M. G. Amin, "Generalized coprime array configurations," presented at the IEEE Sensor Array Multichannel Signal Process. Workshop, A Coruña, Spain, Jun. 2014.
- [3] R. O. Schmidt, "Multiple emitter location and signal parameter estimation," *IEEE Trans. Antennas Propag.*, vol. 34, no. 3, pp. 276–280, Mar. 1986.
- [4] R. Roy and T. Kailath, "ESPRIT—Estimation of signal parameters via rotation invariance techniques," *IEEE Trans. Acoust., Speech, Signal Process.*, vol. 17, no. 7, pp. 984–995, July 1989.
- [5] S. Pillai, *Array Signal Processing*. New York, NY, USA: Springer, 1989.
- [6] R. T. Hoctor and S. A. Kassam, "The unifying role of the co-array in aperture synthesis for coherent and incoherent imaging," *Proc. IEEE*, vol. 78, no. 4, pp. 735–752, Apr. 1990.
- [7] A. Moffet, "Minimum-redundancy linear arrays," *IEEE Trans. Antennas Propag.*, vol. 16, no. 2, pp. 172–175, Mar. 1968.
- [8] G. S. Bloom and S. W. Golomb, "Application of numbered undirected graphs," *Proc. IEEE*, vol. 65, no. 4, pp. 562–570, April 1977.
- [9] P. Pal and P. P. Vaidyanathan, "Nested arrays: A novel approach to array processing with enhanced degrees of freedom," *IEEE Trans. Signal Process.*, vol. 58, no. 8, pp. 4167–4181, Aug. 2010.
- [10] I. J. Gupta and A. A. Ksienski, "Effect of mutual coupling on the performance of adaptive arrays," *IEEE Trans. Antennas Propag.*, vol. AP-31, no. 5, pp. 785–791, Sep. 1983.
- [11] Y. Zhang, K. Hirasawa, and K. Fujimoto, "Signal bandwidth consideration of mutual coupling effects on adaptive array performance," *IEEE Trans. Antennas Propag.*, vol. AP-35, no. 3, pp. 337–339, Mar. 1987.
- [12] P. P. Vaidyanathan and P. Pal, "Sparse sensing with co-prime samplers and arrays," *IEEE Trans. Signal Process.*, vol. 59, no. 2, pp. 573–586, Feb. 2011.
- [13] P. Pal and P. P. Vaidyanathan, "Coprime sampling and the MUSIC algorithm," presented at the IEEE Digit. Signal Process. Workshop/IEEE Signal Process. Educ. Workshop, Sedona, AZ, USA, Jan. 2011.
- [14] W. C. Barott and P. G. Steffes, "Grating lobe reduction in aperiodic linear arrays of physically large antennas," *IEEE Antennas Wireless Propag. Lett.*, vol. 8, pp. 406–408, 2009.
- [15] Y. Rahmat-Samii, *Reflector Antennas*, ser. Antenna Engineering Handbook, Fourth Edition, J. L. Volakis, Ed. New York, NY, USA: McGraw-Hill, 2007, ch. 15.
- [16] Q. Shen, W. Liu, W. Cui, S. W. Y. D. Zhang, and M. G. Amin, "Group sparsity based wideband DOA estimation for co-prime arrays," presented at the IEEE China Summit/Int. Conf. Signal Inf. Process., Xi'an, China, Jul. 2014.
- [17] Y. D. Zhang, M. G. Amin, F. Ahmad, and B. Himed, "DOA estimation using a sparse uniform linear array with two CW signals of co-prime frequencies," in *Proc. IEEE Int. Workshop Comput. Adv. Multi-Sensor Adapt. Process.*, Saint Martin, Dec. 2013, pp. 404–407.
- [18] S. Qin, Y. D. Zhang, and M. G. Amin, "DOA estimation exploiting coprime frequencies," in *Proc. SPIE Wireless Sens., Localization, Process. Conf.*, Baltimore, MD, USA, May 2014, vol. 9103, pp. 91030E1–91030E7.
- [19] T.-J. Shan, M. Wax, and T. Kailath, "On spatial smoothing for direction-of-arrival estimation of coherent signals," *IEEE Trans. Acoust., Speech Signal Process.*, vol. 33, no. 4, pp. 806–811, Aug. 1985.
- [20] B. Friedlander and A. J. Weiss, "Direction finding using spatial smoothing with interpolated arrays," *IEEE Trans. Aerosp., Electron. Syst.*, vol. 28, pp. 574–587, Apr. 1992.
- [21] S. U. Pillai and B. H. Kwon, "Forward/backward spatial smoothing techniques for coherent signal identification," *IEEE Trans. Acoust., Speech Signal Process.*, vol. 37, no. 1, pp. 8–15, Jan. 1989.
- [22] P. Pal and P. P. Vaidyanathan, "On application of LASSO for sparse support recovery with imperfect correlation awareness," presented at the Proc. Asilomar Conf. Signals, Syst., Comput., Pacific Grove, CA, USA, Nov. 2012.
- [23] Y. D. Zhang, M. G. Amin, and B. Himed, "Sparsity-based DOA estimation using co-prime arrays," in *Proc. IEEE ICASSP*, Vancouver, Canada, May 2013, pp. 3967–3971.
- [24] R. Tibshirani, "Regression shrinkage and selection via the lasso," *J. Roy. Statist. Soc.*, ser. Series B, vol. 58, no. 1, pp. 267–288, 1996.

- [25] S. S. Chen, D. L. Donoho, and M. A. Saunders, "Atomic decomposition by basis pursuit," *SIAM J. Sci. Comput.*, vol. 20, no. 1, pp. 33–61, 1998.
- [26] J. A. Tropp and A. C. Gilbert, "Signal recovery from random measurements via orthogonal matching pursuit," *IEEE Trans. Inf. Theory*, vol. 53, no. 12, pp. 4655–4666, 2007.
- [27] S. Ji, D. Dunson, and L. Carin, "Multi-task compressive sampling," *IEEE Trans. Signal Process.*, vol. 57, no. 1, pp. 92–106, Jan. 2009.
- [28] Q. Wu, Y. D. Zhang, M. G. Amin, and B. Himed, "Complex multi-task Bayesian compressive sensing," in *Proc. IEEE ICASSP*, Florence, Italy, May 2014, pp. 3375–3379.
- [29] D. P. Bertsekas, *Nonlinear Programming*, 2nd ed. Belmont, MA, USA: Athena Scientific, 1999.
- [30] P. P. Vaidyanathan and P. Pal, "Sparse sensing with coprime arrays," in *Proc. Asilomar Conf. Signals, Syst., Comput.*, Pacific Grove, CA, USA, Nov. 2010.



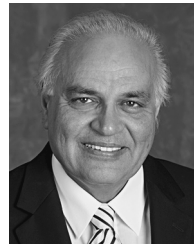
Si Qin received the B.S. and M.S. degrees in Electrical Engineering from Nanjing University of Science and Technology, Nanjing, China, in 2010 and 2013, respectively. Currently, he is a Research Assistant at the Center for Advanced Communications, Villanova University, Villanova, PA, working toward his Ph.D. degree in Electrical Engineering. His research interests include direction-of-arrival estimation, sparse array and signal processing, and radar signal processing.



Yimin D. Zhang (SM'01) received his Ph.D. degree from the University of Tsukuba, Tsukuba, Japan, in 1988. He joined the faculty of the Department of Radio Engineering, Southeast University, Nanjing, China, in 1988. He served as a Director and Technical Manager at the Oriental Science Laboratory, Yokohama, Japan, from 1989 to 1995, and a Senior Technical Manager at the Communication Laboratory Japan, Kawasaki, Japan, from 1995 to 1997. He was a Visiting Researcher at the ATR Adaptive Communications Research Laboratories, Kyoto, Japan, from 1997 to 1998. Since 1998, he has been with the Villanova University, Villanova, PA, where he is currently a Research Professor with the Center for Advanced Communications, and is the Director of the Wireless Communications and Positioning Laboratory and the Director of the Radio Frequency Identification (RFID) Laboratory. His general research interests lie in the areas of statistical signal and array processing applied for radar, communications, and navigation, including compressive sensing, convex optimization, time-frequency analysis, MIMO system, radar imaging, target localization and tracking, wireless networks, and jammer suppression. He has published more than 200 journal articles and peer-reviewed conference papers and 11 book chapters.

Dr. Zhang serves on the Editorial Board of the *Signal Processing* journal. He was an Associate Editor for the IEEE TRANSACTIONS ON SIGNAL PROCESSING during 2010–2014, an Associate Editor for the IEEE SIGNAL PROCESSING LETTERS during 2006–2010, and an Associate Editor for the *Journal of the Franklin Institute* during 2007–2013. He is a member of the IEEE Signal Processing Society's Sensor Array and Multichannel Technical Committee. He

is a Technical Committee Co-chair of the IEEE Benjamin Franklin Symposium on Microwave and Antenna Sub-systems in 2014 and 2015.



Moeness G. Amin (F'01) received his Ph.D. degree in Electrical Engineering from University of Colorado in 1984. He has been on the Faculty of the Department of Electrical and Computer Engineering at Villanova University since 1985. In 2002, he became the Director of the Center for Advanced Communications, College of Engineering. He is a Fellow of the Institute of Electrical and Electronics Engineers (IEEE), 2001; Fellow of the International Society of Optical Engineering, 2007; and a Fellow of the Institute of Engineering and Technology (IET),

2010. Dr. Amin is a Recipient of the IEEE Third Millennium Medal, 2000; Recipient of the 2014 IEEE Signal Processing Society Technical Achievement Award; Recipient of the 2009 Individual Technical Achievement Award from the European Association of Signal Processing; Recipient of the 2010 NATO Scientific Achievement Award; Recipient of the Chief of Naval Research Challenge Award, 2010; Recipient of Villanova University Outstanding Faculty Research Award, 1997; and the Recipient of the IEEE Philadelphia Section Award, 1997. He was a Distinguished Lecturer of the IEEE Signal Processing Society, 2003–2004, and is currently the Chair of the Electrical Cluster of the Franklin Institute Committee on Science and the Arts. Dr. Amin has over 700 journal and conference publications in the areas of Wireless Communications, Time-Frequency Analysis, Sensor Array Processing, Waveform Design and Diversity, Interference Cancellation in Broadband Communication Platforms, satellite Navigations, Target Localization and Tracking, Direction Finding, Channel Diversity and Equalization, Ultrasound Imaging and Radar Signal Processing. He co-authored 18 book chapters. He is the Editor of the two books *Through the Wall Radar Imaging* and *Compressive Sensing for Urban Radar*, published by CRC Press in 2011 and 2014, respectively.

Dr. Amin currently serves on the Editorial Board of the *IEEE Signal Processing Magazine*. He also serves on the Editorial Board of the *Signal Processing* journal. He was a Plenary Speaker at ISSPIT-2003, ICASSP-2010, ACES-2013, IET-2013, EUSIPCO-2013, STATOS-2013, CAMSAP-2013 and RADAR-2014. Dr. Amin was the Special Session Co-Chair of the 2008 IEEE International Conference on Acoustics, Speech, and Signal Processing; the Technical Program Chair of the 2nd IEEE International Symposium on Signal Processing and Information Technology, 2002; the General and Organization Chair of both the IEEE Workshop on Statistical Signal and Array Processing, 2000 and the IEEE International Symposium on Time-Frequency and Time-Scale Analysis, 1994. He was an Associate Editor of the IEEE TRANSACTIONS ON SIGNAL PROCESSING during 1996–1998; a member of the IEEE Signal Processing Society Technical Committee on Signal Processing for Communications during 1998–2002; a Member of the IEEE Signal Processing Society Technical Committee on Statistical Signal and Array Processing during 1995–1997. Dr. Amin was the Guest Editor of the *Journal of Franklin Institute* September-2008 Special Issue on Advances in Indoor Radar Imaging; a Guest Editor of the IEEE TRANSACTIONS ON GEOSCIENCE AND REMOTE SENSING May-2009 Special Issue on Remote Sensing of Building Interior; a Guest Editor of the *IET Signal Processing* December-2009 Special Issue on Time-Frequency Approach to Radar Detection, Imaging, and Classification; a Guest Editor of the *IEEE Signal Processing Magazine* November-2013 and July-2014 Special Issues on Time-frequency Analysis and Applications and Recent Advances in Synthetic Aperture Radar Imaging; and a Guest Editor of the *EURASIP Journal on Advances in Signal Processing* Special Issue on Sparse Sensing in Radar and Sonar Signal Processing.